

# Similarity states of passive scalar transport in buoyancy-generated turbulence

J. R. Chasnov

The Hong Kong University of Science and Technology, Clear Water Bay, Kowloon, Hong Kong

(Received 23 June 1994; accepted 14 February 1995)

The mixing of a passive scalar field by turbulence that is generated by buoyancy forces acting on an initial random density field is considered. Various asymptotic similarity states of the passive scalar field with and without a uniform mean passive scalar gradient are determined by dimensional arguments based on exact or near invariants of the density and passive scalar fields. The results of large-eddy numerical simulations are shown to support the derived scaling laws. The large-eddy simulations also demonstrate the different mixing properties of an active and passive scalar field. © 1995 American Institute of Physics.

## I. INTRODUCTION

The time-decay exponent of the kinetic energy per unit mass of a high Reynolds number isotropic turbulence can be predicted by assuming the existence of an asymptotic similarity state based on an invariant of the flow field.<sup>1-4</sup> An analogous result may also be obtained for the time-decay exponent of the scalar variance of a decaying high Péclet number isotropic passive scalar field.<sup>5,6</sup> Recent works have demonstrated a wider existence of asymptotic similarity states for homogeneous turbulence than hitherto suspected. In particular, asymptotic similarity states of the velocity and/or scalar field were discovered in recent studies of buoyancy-generated turbulence,<sup>7</sup> decaying isotropic turbulence in a uniform mean passive scalar gradient,<sup>8</sup> decaying axisymmetric turbulence,<sup>9</sup> stably stratified turbulence,<sup>10</sup> and rotating turbulence.<sup>11</sup>

In this paper we return to the study of buoyancy-generated turbulence, where velocity fluctuations are assumed to be created in a fluid initially at rest by buoyancy forces acting on a random distribution of fluid density. Previously, an invariant of the density field was discovered which led to the prediction of asymptotic similarity states of both the velocity and density fields. We now further consider the mixing of an additional passive scalar field transported by the buoyancy-generated velocity fluctuations. Such a physical flow may occur, say, if a random initial temperature field is created by some means in a large body of fluid at rest. In addition to the buoyant random temperature fluctuations, there may be another random concentration field such as salinity which negligibly affects the fluid density. We ask whether asymptotic similarity states of this additional passive scalar field may also exist? We will show that indeed similarity states do exist, and that they too can be based on the invariant of the density field. We do not yet know of any laboratory experiments on buoyancy-generated turbulence, nor of any relevant observational data. Our primary motivation for studying this problem is to demonstrate further the general appearance of asymptotic similarity states in freely-evolving homogeneous turbulence. Furthermore, this hypothetical flow serves the additional purpose of illustrating the different turbulent mixing properties of an active and passive scalar field under relatively simple conditions.

We will separately consider two distinct physical scenarios for the passive scalar field. In both cases, fluctuations in the density of the fluid (the active scalar) are created at the initial instant, and velocity fluctuations are subsequently generated by buoyancy forces. In the first case, fluctuations in another passive scalar field (assumed not to affect the fluid velocity) are also created at the initial instant. The generated velocity fluctuations subsequently mix both the active and passive scalar fields. In the second case, a uniform mean passive scalar gradient is imposed across the fluid. The generated velocity fluctuations along the direction of the gradient subsequently generate passive scalar fluctuations, which are then mixed by the buoyancy-generated velocity field. The transport of passive scalar fields with and without a uniform mean gradient was also considered previously,<sup>8</sup> the difference here being that the decaying isotropic velocity field considered earlier is replaced by a buoyancy-generated flow field.

## II. THE GOVERNING EQUATIONS

The equations which govern the evolution of our velocity and density fields may be obtained upon use of the well-known Boussinesq approximation that small density fluctuations affect the flow only through the buoyancy force:

$$\nabla \cdot \mathbf{u} = 0, \quad (1)$$

$$\frac{\partial \mathbf{u}}{\partial t} + \mathbf{u} \cdot \nabla \mathbf{u} = \frac{\rho' \mathbf{g}}{\rho_0} - \frac{\nabla(p - \rho_0 \mathbf{g} \cdot \mathbf{x})}{\rho_0} + \nu \nabla^2 \mathbf{u}, \quad (2)$$

$$\frac{\partial \rho'}{\partial t} + \mathbf{u} \cdot \nabla \rho' = D \nabla^2 \rho', \quad (3)$$

where  $\mathbf{u}$ ,  $p$ , and  $\nu$  are the fluid velocity, pressure, and kinematic viscosity,  $\rho_0$  is the constant mean value of the fluid density, and  $\rho'$  is its fluctuation about the mean,  $\mathbf{g} = -j\mathbf{g}$ , where  $g > 0$  is the gravitational acceleration and  $j$  is the vertical (upwards) unit vector, and  $D$  is the diffusivity of the quantity which is resulting in the fluctuation of the fluid density. Denoting the passive scalar field by  $\theta$ , its transport equation may be written as

$$\frac{\partial \theta}{\partial t} + \mathbf{u} \cdot \nabla \theta = -\beta \cdot \mathbf{u} + D_\theta \nabla^2 \theta, \quad (4)$$

where  $\beta$  is the constant mean scalar gradient (possibly zero) in some as yet unspecified direction, and  $D_\theta$  is the molecular diffusivity of the additional passive scalar field. We have assumed that the fluid density is negligibly affected by fluctuations in this scalar field. When  $\beta=0$ , the equation for the passive scalar is identical to that for the density field, apart from the possible difference in the diffusion coefficients which will be inconsequential at the large Péclet numbers of interest to us here. To allow the passive scalar to evolve differently than the density field, we make the physically reasonable assumption that the correlation  $\langle \rho' \theta \rangle = 0$  at the initial instant. It is easy to show directly from the governing equations that this correlation subsequently remains zero for all times. We will further assume different statistical forms for the initial density and passive scalar distributions, as described in the next section.

### III. THE LARGE-SCALE FIELDS

At the initial instant,  $t=0$ , the fluid is at rest so that  $\mathbf{u}(\mathbf{x})=0$  everywhere, and the density field  $\rho'(\mathbf{x})$  is a random statistically isotropic realization of some given initial spectrum. If we reasonably assume that the three-dimensional spectrum of the density fluctuations  $\Psi_\rho(\mathbf{k}, t)$  [the Fourier transform of the density covariance  $\langle \rho'(\mathbf{x})\rho'(\mathbf{x}+\mathbf{r}) \rangle$ , where  $\langle \dots \rangle$  denotes an ensemble, or volume average] is an even function of  $k$ , then the spherically-integrated spectrum  $E_\rho(k, t)$ , defined so that its integral over  $k$  is one-half the density variance, has one of the following forms near  $k=0$  for  $t>0$ :

$$E_\rho(k, t) \sim 2\pi C_0 k^2 \quad \text{or} \quad E_\rho(k, t) \sim 2\pi C_2(t) k^4. \quad (5)$$

The  $k^2$  coefficient  $C_0$  has been shown to be an invariant of the flow,<sup>5</sup> with its value at all times equal to its value at  $t=0$ . When  $C_0$  is zero initially, it can be shown within a quasilinear approximation that a positive increasing value of  $C_2$  is generated by nonlinear interactions.<sup>12</sup>

Similar comments also apply to the three-dimensional spectrum of the passive scalar fluctuations  $\Psi_\theta(\mathbf{k}, t)$  and the corresponding spherically integrated spectrum  $E_\theta(k, t)$ . When  $\beta=0$ ,  $E_\theta(k, t)$  thus has one of the following forms near  $k=0$  for  $t>0$ :

$$E_\theta(k, t) \sim 2\pi A_0 k^2 \quad \text{or} \quad E_\theta(k, t) \sim 2\pi A_2(t) k^4, \quad (6)$$

where  $A_0$  is strictly invariant; when  $A_0=0$ , a nonzero value of  $A_2$  is generated by nonlinear interactions.

With the density-variance spectrum following one of (5) near  $k=0$ , the corresponding form of the buoyancy-generated kinetic energy spectrum  $E(k, t)$  near  $k=0$  is

$$E(k, t) \sim 2\pi B_0(t) k^2 \quad \text{or} \quad E(k, t) \sim 2\pi B_2(t) k^4, \quad (7)$$

respectively, where an exact result for  $B_0(t)$  may be obtained from the governing equations. First, defining the velocity spectral tensor  $\Phi_{ij}$  to be the Fourier transform of the velocity covariance  $\langle u_i(\mathbf{x})u_j(\mathbf{x}+\mathbf{r}) \rangle$ , and considering its behavior near  $k=0$ , one finds

$$\Phi_{ij}(\mathbf{k}) = \left(\frac{g}{\rho_0}\right)^2 \left(\delta_{i3} - \frac{k_i k_3}{k^2}\right) \left(\delta_{j3} - \frac{k_j k_3}{k^2}\right) C_0 t^2 + O(1), \quad (8)$$

where  $O(1)$  represents terms which vanish when  $k \rightarrow 0$ , and  $C_0$  is the (invariant) value of the density spectral function at  $k=0$ . The initial large-scale density fluctuation is assumed to be isotropic. Equation (8) is in agreement with the work of Saffman<sup>3</sup> for fluid motion generated by a nonsolenoidal force such as gravity, except that here the force is applied continuously rather than only at the initial instant. The exact time dependence of the energy spectral coefficient  $B_0$  is determined from (8) by setting  $i=j$  and summing, averaging over the directions of  $\mathbf{k}$  and taking  $k=0$ :

$$B_0(t) = \frac{2}{3} \left(\frac{g^2 C_0}{\rho_0^2}\right) t^2. \quad (9)$$

With a nonzero value for  $\beta$  and zero initial passive scalar fluctuations, the behavior of the  $k^2$  coefficient  $A_0$  of the passive scalar spectrum near  $k=0$  becomes an explicit function of time which may also be determined exactly. We consider here explicitly a mean passive scalar gradient  $\beta$  along the vertical direction. The results are easily generalized to  $\beta$  in an arbitrary direction. For  $\beta$  along  $\mathbf{j}$ , we determine

$$\Psi_\theta(\mathbf{k}) = \frac{1}{4} \left(\frac{g\beta}{\rho_0}\right)^2 \left(1 - \frac{k_3^2}{k^2}\right)^2 C_0 t^4 + O(1), \quad (10)$$

which may be further averaged over the directions of  $\mathbf{k}$  to obtain the exact result

$$A_0(t) = \frac{2}{15} \left(\frac{g^2 \beta^2 C_0}{\rho_0^2}\right) t^4. \quad (11)$$

The value of  $A_0$  when  $\beta$  is perpendicular to  $\mathbf{j}$  is found to be a factor of 8 smaller than (11).

### IV. EXACT ASYMPTOTIC SIMILARITY STATES

We are now in a position to determine exact asymptotic similarity states of a passive scalar field in buoyancy-generated turbulence when the large-scale density fluctuations are characterized by a nonzero  $C_0$ . We begin with dimensionally correct forms of the evolution of the mean-square velocity, density variance and integral scale in a high Reynolds and Péclet number turbulence:<sup>8</sup>

$$\langle \mathbf{u}^2 \rangle \propto B_0^{2/5} t^{-6/5}, \quad \langle \rho'^2 \rangle \propto C_0 B_0^{-3/5} t^{-6/5}, \quad l \propto B_0^{1/5} t^{2/5}. \quad (12)$$

For a buoyancy-generated flow field, we replace  $B_0=B_0(t)$  with (9) to find the laws

$$\langle \mathbf{u}^2 \rangle \propto \left(\frac{g^2 C_0}{\rho_0^2}\right)^{2/5} t^{-2/5},$$

$$\langle \rho'^2 \rangle \propto C_0 \left(\frac{g^2 C_0}{\rho_0^2}\right)^{-3/5} t^{-12/5}, \quad l \propto \left(\frac{g^2 C_0}{\rho_0^2}\right)^{1/5} t^{4/5} \quad (13)$$

in agreement with earlier work.<sup>7</sup> Also observe the interesting feature that the Reynolds number of the flow field increases asymptotically as  $t^{3/5}$ . Now, when  $\beta=0$ , the evolution of the passive scalar variance may also be found from (12) upon replacing  $B_0$  with (9) once again, and  $C_0$  with  $A_0$ :

$$\langle \theta^2 \rangle \propto A_0 \left(\frac{g^2 C_0}{\rho_0^2}\right)^{-3/5} t^{-12/5}. \quad (14)$$

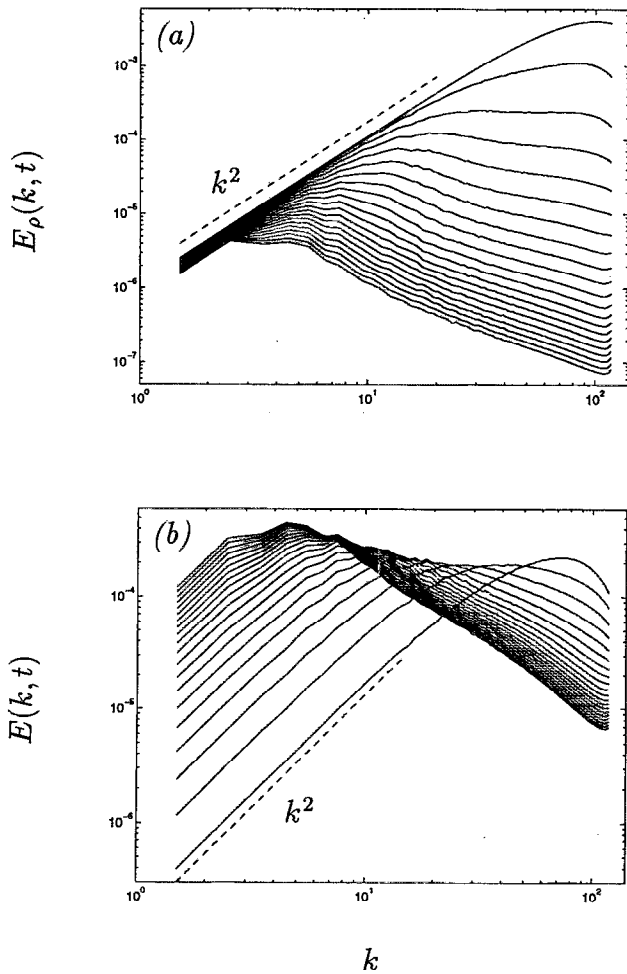


FIG. 1. Time evolution of the density and energy spectra with  $E_\rho(k, t) \sim k^2$  near  $k=0$ : (a) density spectrum  $E_\rho(k, t)$ ; (b) energy spectrum  $E(k, t)$ .

We have thus obtained the result that a passive scalar field initialized with  $A_0$  nonzero decays asymptotically at the same rate as the density field with  $C_0$  nonzero. Note that there are undetermined dimensionless coefficients in (13) and (14), and it is reasonable to expect that the coefficient in the scaling equation for  $\langle \rho'^2 \rangle$  will be smaller than the coefficient in the equation for  $\langle \theta^2 \rangle$  since the mixing of density fluctuations should be more efficient than the mixing of a passive scalar. Large magnitude density fluctuations generate vertical velocity fluctuations directly at the location where mixing can be most effective.

For the passive scalar with nonzero mean scalar gradient ( $\beta \neq 0$ ), there exists only the single invariant low wavenumber density spectral coefficient. Replacing  $A_0 = A_0(t)$  in (14) by (11), the passive scalar variance is determined to increase asymptotically as

$$\langle \theta^2 \rangle \propto \beta^2 \left( \frac{g^2 C_0}{\rho_0} \right)^{2/5} t^{8/5}. \quad (15)$$

For a passive scalar field with uniform mean gradient in a decaying isotropic turbulence, we previously<sup>8</sup> determined a slower increase with power-law exponent  $t^{4/5}$ . Buoyancy-generated turbulence is hence significantly more effective in

generating passive scalar fluctuations from a uniform mean gradient than is an isotropically decaying turbulence.

For comparison with our later numerical simulations, we now construct exact asymptotic similarity states for the passive scalar spectra. Similarity states have previously<sup>7</sup> been constructed for the density and energy spectra and we also

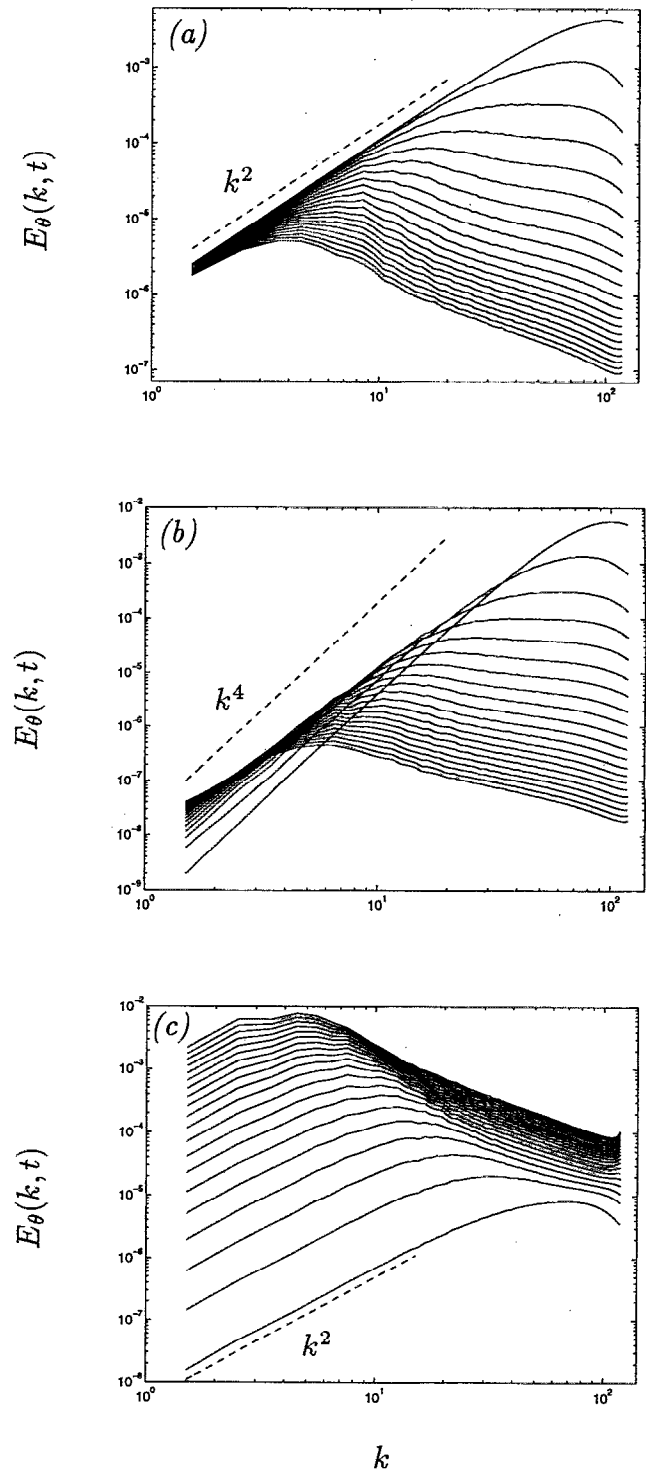


FIG. 2. Time evolution of the passive scalar spectra  $E_\theta(k, t)$  corresponding to the density and energy spectra of Fig. 1: (a)  $E_\theta \sim k^2$  near  $k=0$ ; (b)  $E_\theta \sim k^4$  near  $k=0$ ; (c)  $E_\theta$  with  $\beta|g$ .

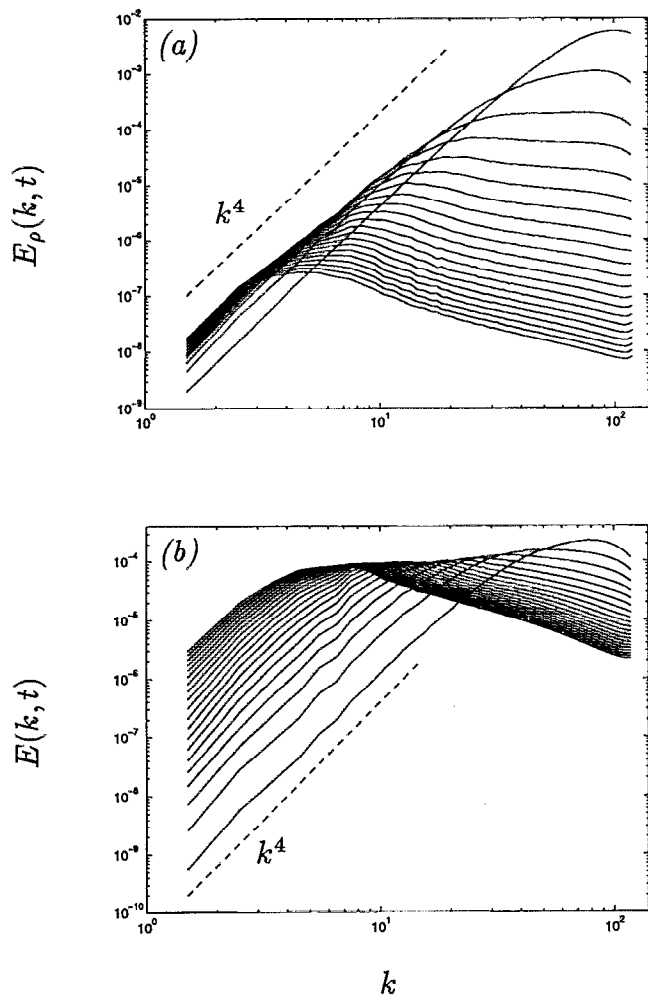


FIG. 3. Time evolution of the density and energy spectra with  $E_\rho(k, t) \sim k^4$  near  $k=0$ : (a) density spectrum  $E_\rho(k, t)$ ; (b) energy spectrum  $E(k, t)$ .

include them here for completeness. Using the results of (13) and (14), the similarity forms of the energy, density, and decaying passive scalar spectra are determined to be

$$E(k, t) = \left( \frac{g^2 C_0}{\rho_0^2} \right)^{3/5} t^{2/5} \hat{E}(\hat{k}), \quad (16)$$

$$E_\rho(k, t) = C_0 \left( \frac{g^2 C_0}{\rho_0^2} \right)^{-2/5} t^{-8/5} \hat{E}_\rho(\hat{k}); \quad (17)$$

$$E_\theta(k, t) = A_0 \left( \frac{g^2 C_0}{\rho_0^2} \right)^{-2/5} t^{-8/5} \hat{E}_\theta(\hat{k}). \quad (17)$$

In the presence of a uniform passive scalar gradient, the corresponding similarity state for the passive scalar spectrum is

$$E_\theta(k, t) = \beta^2 \left( \frac{g^2 C_0}{\rho_0^2} \right)^{3/5} t^{12/5} \hat{E}_\theta(\hat{k}). \quad (18)$$

The nondimensional wave number  $\hat{k}$  is given by

$$\hat{k} = \left( \frac{g^2 C_0}{\rho_0^2} \right)^{1/5} t^{4/5} k. \quad (19)$$

## V. OTHER POSSIBLE SIMILARITY STATES

When  $A_0$  and/or  $C_0$  are initially zero, there no longer exist exact invariants on which to base asymptotic similarity states. Nevertheless, earlier numerical results<sup>7,8</sup> suggest the development of other similarity states and that approximate forms for these similarity states may be obtained by assum-

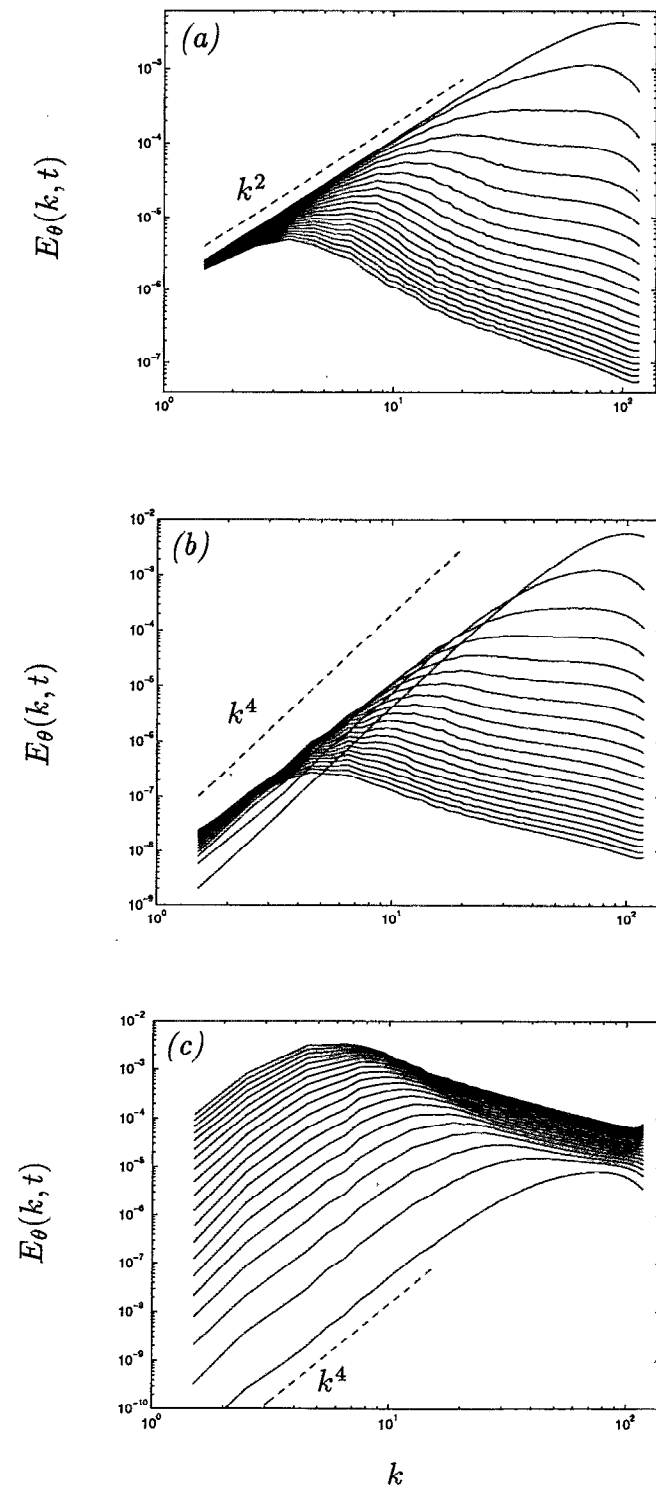


FIG. 4. Time evolution of the passive scalar spectra  $E_\theta(k, t)$  corresponding to the density and energy spectra of Fig. 3: (a)  $E_\theta \sim k^2$  near  $k=0$ ; (b)  $E_\theta \sim k^4$  near  $k=0$ ; (c)  $E_\theta$  with  $\beta||g$ .

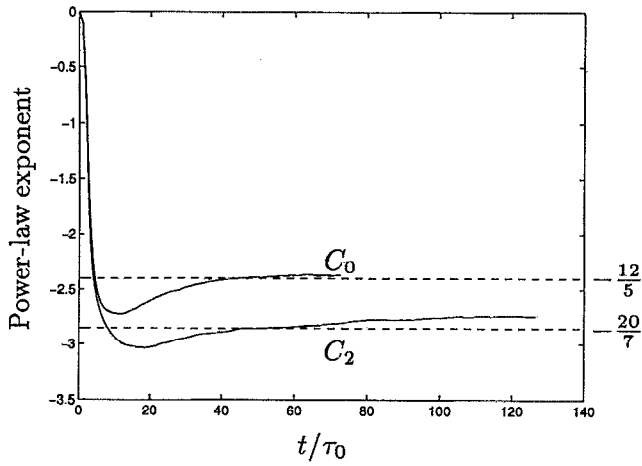


FIG. 5. Time evolution of the power-law exponent of  $\langle \rho'^2 \rangle$ . The solid lines are the results of the large-eddy simulations and the dashed lines are the exact and approximate analytical results discussed in Secs. IV and V.

ing the near invariance of the coefficient  $A_2$ , and that of  $C_2$  when  $\beta=0$ . These theoretical results are necessarily less certain, since the exact time dependence of  $A_2$ ,  $B_2$ , and  $C_2$  can not at present be accurately estimated without direct solution of the governing equations,<sup>13</sup> or some type of closure approximation.<sup>14</sup>

When  $C_0 \neq 0$ , an approximate solution may be obtained for a decaying passive scalar field ( $\beta=0$ ) with  $A_0=0$  initially:

$$\langle \theta^2 \rangle \propto A_2 \left( \frac{g^2 C_0}{\rho_0^2} \right)^{-1} t^{-4}, \quad (20)$$

where we assume that  $A_2$  is nearly invariant at large times.

Other approximate solutions may be obtained when  $C_0=0$  initially by assuming that  $C_2$  is nearly invariant at large times. Previously, approximate results were obtained

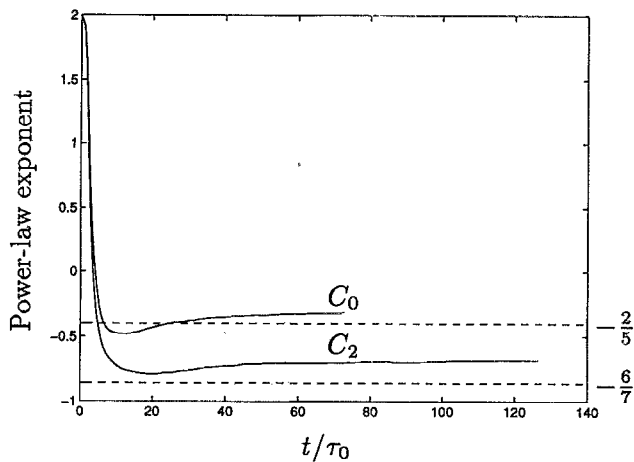


FIG. 6. Time evolution of the power-law exponent of  $\langle \mathbf{u}^2 \rangle$ . The solid lines are the results of the large-eddy simulations and the dashed lines are the exact and approximate analytical results discussed in Secs. IV and V.

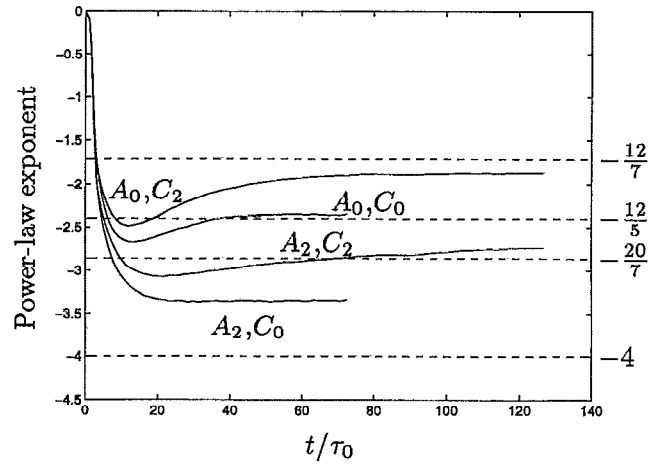


FIG. 7. Time evolution of the power-law exponent of  $\langle \theta^2 \rangle$  with  $\beta=0$ . The solid lines are the results of the large-eddy simulations and the dashed lines are the exact and approximate analytical results discussed in Secs. IV and V.

for the evolution of the density variance, mean-square velocity fluctuation, and integral scale in the buoyancy-generated flow:<sup>7</sup>

$$\begin{aligned} \langle \mathbf{u}^2 \rangle &\propto \left( \frac{g^2 C_2}{\rho_0^2} \right)^{2/7} t^{-6/7}, \\ \langle \rho'^2 \rangle &\propto C_2 \left( \frac{g^2 C_2}{\rho_0^2} \right)^{-5/7} t^{-20/7}, \quad l \propto \left( \frac{g^2 C_2}{\rho_0^2} \right)^{1/7} t^{4/7}. \end{aligned} \quad (21)$$

Two more approximate similarity states for a decaying passive scalar field with  $\beta=0$  may also be determined:

$$\langle \theta^2 \rangle \propto A_0 \left( \frac{g^2 C_2}{\rho_0^2} \right)^{-3/7} t^{-12/7} \quad \text{or} \quad A_2 \left( \frac{g^2 C_2}{\rho_0^2} \right)^{-5/7} t^{-20/7}, \quad (22)$$

depending on whether  $A_0$  is nonzero, or zero, initially. Note that the second of Eq. (22) exhibits the same time dependence as that of the density field in that flow.

Finally, for a passive scalar field with  $\beta \neq 0$ , the approximate solution when  $C_0=0$  initially is given by

$$\langle \theta^2 \rangle \propto \beta^2 \left( \frac{g^2 C_2}{\rho_0^2} \right)^{2/7} t^{8/7}. \quad (23)$$

Equation (23) is to be compared to the time dependence  $t^{4/7}$  found previously<sup>8</sup> when the hydrodynamics is that of decaying isotropic turbulence with  $B_0=0$ .

Closure calculations for isotropic turbulence<sup>14</sup> suggest the possibility that (20)–(23) may in fact be exact provided we use the precise values of  $A_2=A_2(t)$  and  $C_2=C_2(t)$ . We can test this hypothesis by constructing the following possible asymptotic similarity forms for the various spectra:

$$\begin{aligned} E(k, t) &= \langle \mathbf{u}^2 \rangle l \hat{E}(\hat{k}), & E_\rho(k, t) &= \langle \rho'^2 \rangle l \hat{E}_\rho(\hat{k}), \\ E_\theta(k, t) &= \langle \theta^2 \rangle l \hat{E}_\theta(\hat{k}), & \hat{k} &= lk. \end{aligned} \quad (24)$$

The numerical values of  $\langle \mathbf{u}^2 \rangle$ ,  $\langle \theta^2 \rangle$  and the integral scale  $l$  may be taken directly from the large-eddy simulations. The integral scales of the various fields are all expected to grow at the same rate; however, in rescaling the spectra we will

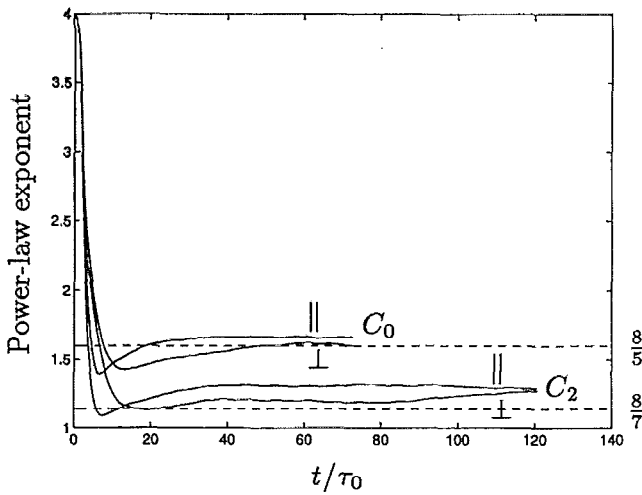


FIG. 8. Time evolution of the power-law exponent of  $\langle \theta^2 \rangle$  with  $\beta=1$ . The solid lines are the results of the large-eddy simulations and the dashed lines are the exact and approximate analytical results discussed in Secs. IV and V.

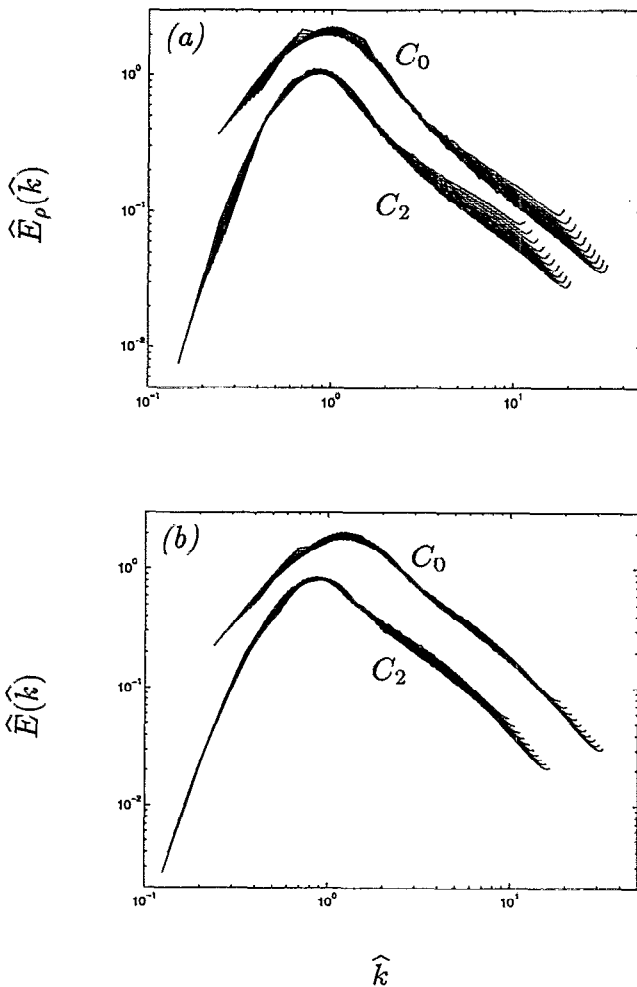


FIG. 9. Rescaling of the last ten spectra in each of Figs. 1 and 3 according to the similarity forms given in Secs. IV and V: (a) density spectrum  $E_\rho(k,t)$ ; (b) energy spectrum  $E(k,t)$ .

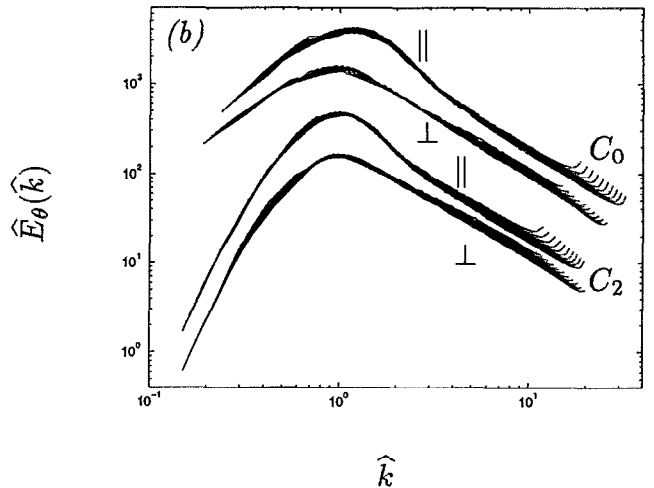
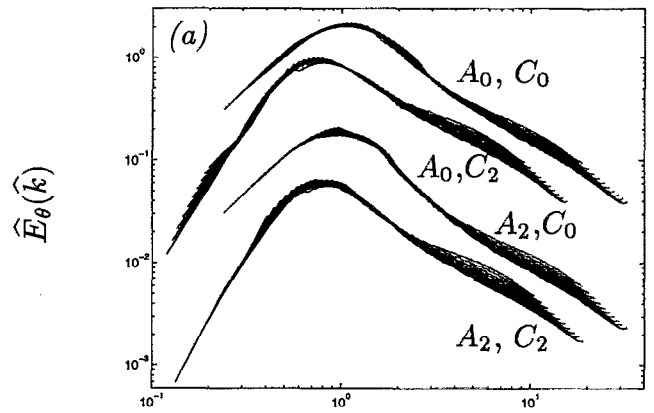


FIG. 10. Rescaling of the last ten spectra in each of Figs. 2 and 4 according to the similarity forms given in Secs. IV and V: (a)  $\beta=0$ ; (b)  $\beta=1$ .

use the spherically averaged integral scale associated with the given field. The similarity forms given by (24) generalize (16)–(19) when there no longer exists exact invariants.

## VI. LARGE-EDDY SIMULATIONS

In this section, we present the results of large-eddy simulations used to test the similarity state predictions of Secs. IV and V, and to compute dimensionless coefficients of interest which can not be predicted *a priori*. The numerical simulations presented here are similar to those done previously.<sup>7,8</sup> A parallel pseudospectral code<sup>15,16</sup> for turbulence in a periodic box of length  $2\pi$  is used with an eddy viscosity/diffusivity subgrid model<sup>17,18</sup> to solve the velocity, density, and scalar field equations given by (1)–(4). The molecular transport coefficients are set to zero. Here, the results of two separate  $256^3$  simulations will be presented, each simulation time evolving a (three-dimensional) velocity field and five scalar fields, which included one active density field, two passive scalar fields with no mean scalar gradient ( $\beta=0$ ), and two passive scalar fields with mean scalar gradient ( $\beta=1$ ) parallel or perpendicular to the gravitational direction. The initial conditions of both simulations were such that the velocity

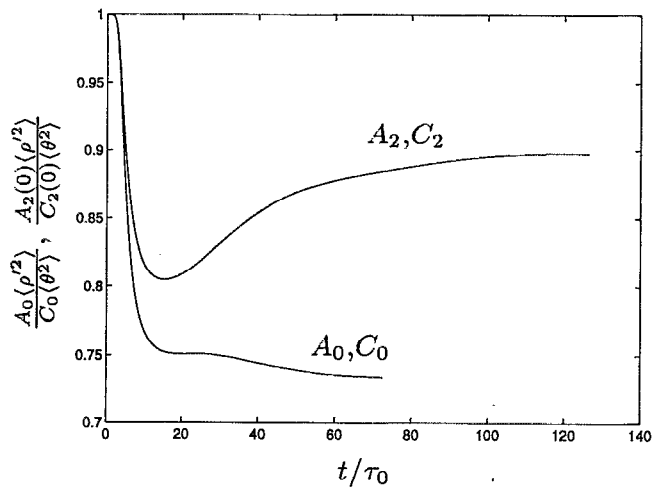


FIG. 11. Comparison of the relative mixing efficiencies of an active and passive scalar field.

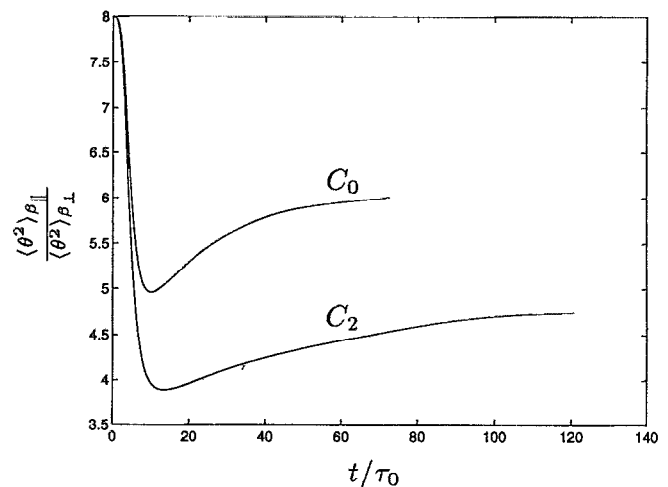


FIG. 12. Ratio of the scalar variance generated for a scalar gradient parallel to the gravitation axis to that generated when the scalar gradient is perpendicular to the axis.

field and the two passive scalar fields with  $\beta=1$  were zero everywhere at the initial instant. The two passive scalar fields with  $\beta=0$  were initialized in both simulations to a  $k^2$  and  $k^4$  spectral behavior near  $k=0$ . The two different simulation runs corresponded to an active density field initialized with either a  $k^2$  or  $k^4$  spectrum near  $k=0$ .

The general form of the initial  $k^2$  and  $k^4$  active and passive scalar spectra is given by

$$E_{\rho, \theta}(k, 0) = \frac{1}{2} a_s \theta_0^2 k_p^{-1} (k/k_p)^s \exp[-\frac{1}{2} s (k/k_p)^2], \quad (25)$$

where  $s$  is equal to 2 or 4 and  $a_s$  is the appropriate normalization constant so that the integral over the spectrum yields  $\langle \theta_0^2 \rangle / 2$ . The initial scalar spectrum is maximum at wave number  $k_p$ . We choose  $\theta_0=1$  and  $k_p=100$ , and set the gravitation coefficient  $g/\rho_0$  to unity. The two simulations performed encompass all of the possible similarity states discussed in Secs. IV and V.

Figures 1 and 2 present the spectral results of the first simulation with  $E_{\rho}(k, t) \sim 2\pi k^2 C_0$  near  $k=0$ . Figure 1 displays the density and energy spectra, previously computed at  $128^3$  resolution in an earlier work.<sup>7</sup> We have been careful to maintain sufficient sample of the energetic eddies at the latest times of evolution. The spectral results for the passive scalar fields are given in Fig. 2: Figs. 2(a) and 2(b) present the decaying spectra for a passive scalar field initialized with a  $k^2$  and  $k^4$  spectrum, respectively, and Fig. 2(c) presents the growing spectrum of the passive scalar field with mean scalar gradient parallel to the axis of gravity. The spectrum of the passive scalar field with mean scalar gradient perpendicular to the axis of gravity is of similar shape, and is omitted here. Figures 3 and 4 present the corresponding spectral results of the second simulation with  $E_{\rho}(k, t) \sim 2\pi k^4 C_2$  near  $k=0$ .

The time evolution of the power-law exponents (logarithmic derivatives) of the density variance resulting from the two simulations is presented in Fig. 5 while those of the root-mean-square (RMS) velocity are presented in Fig. 6. The simulation results are labeled by the leading-order low wave-number spectral coefficient  $C_0$  and  $C_2$ , respectively, of

the density spectrum. The solid lines are the results of the simulations and the dashed lines are the exact and approximate theoretical results discussed in Secs. IV and V. Time is in units of  $\tau_0 = \sqrt{l_0 \rho_0 / g \theta_0}$ , where  $l_0$  is the initial integral scale of the density field, given by  $l_0 = \sqrt{\pi} / k_p$  when  $s=2$  in (25), and  $l_0 = 2\sqrt{2\pi} / 3k_p$  when  $s=4$ . The simulation and theoretical scalings are found to be in good agreement, particularly when the theoretical results are expected to be exact.

The new results of interest to us here—the decay and growth exponents of the passive scalar variance—are presented in Figs. 7 and 8. Figure 7 presents the decay exponents for a decaying passive scalar field with no mean scalar gradient, and Fig. 8 presents the growth exponents of the growing passive scalar field with mean gradient parallel or perpendicular to the gravitational axis. The dashed lines are the exact and approximate theoretical results discussed earlier. In Fig. 7, the simulation curves are labeled by the leading-order low wave-number spectral coefficients of the passive scalar and density field. The exact theoretical result  $-12/5$  for the exponent, obtained when both  $A_0$  and  $C_0$  are nonzero, is in excellent agreement with the corresponding results from the numerical simulation. The remaining approximate theoretical results are in qualitative agreement with the simulation results, with the largest deviation occurring when  $A_2$  and  $C_0$  are the leading-order spectral coefficients. In this case, we obtain an asymptotic power-law exponent of approximately  $-3.35$  instead of  $-4$ , a difference of about 16%. This difference is most likely a consequence of the relatively large time variation of the coefficient  $A_2 = A_2(t)$  in (20).

In Fig. 8, the simulation results are labeled by the leading-order low wave-number spectral coefficient of the density field, and by  $\parallel$  or  $\perp$ , corresponding to a passive scalar gradient parallel or perpendicular to the gravitational field, respectively. The simulation results are also in good agreement with the theoretical predictions. The exponent  $8/5$ , corresponding to a density spectrum proportional to  $k^2$  near

$k=0$ , is expected to be exact and the agreement between the simulations and theoretical result is excellent. The exponent  $8/7$  is only approximate for a density spectrum proportional to  $k^4$  near  $k=0$ , and the simulation results deviate somewhat more from this theoretical result.

The reasonable agreement of the power-law exponents computed above with the theoretical results of Sec. IV and V indicates the overall soundness of our theoretical arguments. Additional evidence for the existence of asymptotic similarity states of the flow fields may be obtained by demonstrating a collapse of the spectra at the latest times of the simulation under the exact similarity scaling of Sec. IV, as well as the similarity scaling of Sec. V given by (24). The latter scaling may also be exact, but the asymptotic behavior of  $\langle \theta^2 \rangle$  and  $l$  are not known *a priori* but are given by the results of the simulation. In Figs. 9(a) and 9(b), the last (in time evolution) ten displayed density and energy spectra shown in Figs. 1 and 3 are rescaled according to the above-mentioned similarity scalings, apart from arbitrary multiplicative constants which just shift the curves on the log-log plots to permit a clearer display. In Figs. 10, the analogous rescaled passive scalar spectra are also plotted. Figures 10(a) and 10(b) correspond to zero and nonzero mean passive scalar gradients, respectively. For  $s=2$  in (25), the nondimensional times displayed range between  $33 < t/\tau_0 < 72$ , while for  $s=4$ ,  $45 < t/\tau_0 < 126$ . The collapse of all the spectra is quite remarkable, indicating that similarity states of the flow field exist even when the low wave-number coefficients are not strictly invariant.

Finally, we present numerical results pertaining to two dimensionless coefficients of interest which can not be predicted by the dimensional arguments of Secs. IV and V. The first coefficient is related to the relative efficiency of turbulence mixing of an active or passive scalar field. We have seen that for density and passive scalar fields of initially the same spectra (but different realizations), the asymptotic rate of decay of density and scalar variance are the same as evidenced by the same decay exponents. However, as noted earlier, the proportionality constants may be different corresponding to different mixing efficiencies. In Fig. 11, we plot the ratio  $A_0 \langle \rho'^2 \rangle / C_0 \langle \theta^2 \rangle$ , when  $A_0$  and  $C_0$  are the leading-order spectral coefficients of the passive scalar and density spectra, respectively; and  $A_2 \langle \rho'^2 \rangle / C_2 \langle \theta^2 \rangle$ , when  $A_2$  and  $C_2$  are the leading-order spectral coefficients. These latter coefficients are taken at  $t=0$ . The computed ratios decrease from unity at the initial instant, indicating more efficient mixing of the density field. The value of the ratio for the  $A_0, C_0$  case decreases to an approximate asymptotic value of 0.75. The value of this ratio for the  $A_2, C_2$  case asymptotes to a higher value of 0.9.

The values of the low wave-number coefficients using in the ratios above are not readily obtainable from experimental measurements. However, they may be related to more easily measurable quantities using the initial spectra given by (25). For instance, the spectral coefficient  $A_0$  is given by

$$A_0 = \frac{\theta_0^2 l_0^3}{\pi^3},$$

where  $\theta_0^2$  is the initial passive scalar variance and  $l_0$  is the

spherically averaged passive scalar integral scale. An analogous result is also obtained for  $C_0$ . When  $A_2$  is the lowest-order coefficient, the scaling on  $l_0^3$  is replaced by  $l_0^5$ .

The other dimensionless coefficient, plotted in Fig. 12, is the ratio of the scalar variance when the uniform mean gradient is along the gravitational axis, to that when the gradient is perpendicular to the axis. At small times, the value of this ratio is eight as can be computed from the linearized equations, and decreases to somewhat smaller values at later times. When  $C_0$  is the leading-order density spectral coefficient, the asymptotic value is approximately 6, while when  $C_2$  is the leading-order coefficient, the asymptotic value is closer to 5.

## VII. CONCLUSIONS

The theoretical results and the results of the large-eddy simulations taken together clearly demonstrate the development of asymptotic similarity states of a passive scalar field transported by homogeneous buoyancy-generated turbulence. Using a simple similarity analysis, we have thus predicted the long-time evolution of a decidedly nontrivial flow—the nonlinear interactions in this system are fairly complex and involve a coupling between the three-dimensional velocity field and both an active and passive scalar field. Direct analytical consideration of the full nonlinear equations by closure, for instance, would have been complicated indeed. We have avoided the need for such a detailed analytical investigation by considering the consequence of the existence of exact and approximate flow invariants associated with the density and passive scalar field. This powerful technique of similarity analysis together with large-eddy simulations hold promise for the discovery of other asymptotic similarity states in homogeneous turbulence.

## ACKNOWLEDGMENTS

I wish to thank Dr. Robert Rogallo and Dr. Alan Wray for the use of their software. The support of the Hong Kong Research Grant Council is gratefully acknowledged. The computations presented here were performed on a 140 node Intel Paragon at The Hong Kong University of Science and Technology.

<sup>1</sup>L. G. Loitsianski, "Some basic laws for isotropic turbulent flow," Tr. Tsentr. Aero.-Giedrodin. Inst. **440**, 31 (1939).

<sup>2</sup>A. N. Kolmogorov, "On degeneration of isotropic turbulence in an incompressible viscous liquid," Dokl. Akad. Nauk. SSSR **31**, 538 (1941).

<sup>3</sup>P. G. Saffman, "The large-scale structure of homogeneous turbulence," J. Fluid Mech. **27**, 581 (1967).

<sup>4</sup>P. G. Saffman, "Note on decay of homogeneous turbulence," Phys. Fluids **10**, 1349 (1967).

<sup>5</sup>S. Corrsin, "The decay of isotropic temperature fluctuations in an isotropic turbulence," J. Aeronaut. Sci. **18**, 417 (1951).

<sup>6</sup>M. Larcheveque, J. P. Chollet, J. R. Herring, M. Lesieur, G. R. Newman, and D. Schertzer, "Two-point closure applied to a passive scalar in decaying isotropic turbulence," in *Turbulent Shear Flows II*, edited by J. S. Bradbury, F. Durst, B. E. Launder, F. W. Schmidt, and J. H. Whitelaw (Springer-Verlag, Berlin, 1980), pp. 50–65.

<sup>7</sup>G. K. Batchelor, V. M. Canuto, and J. R. Chasnov, "Homogeneous buoyancy-generated turbulence," J. Fluid Mech. **235**, 349 (1992).

- <sup>8</sup>J. R. Chasnov, "Similarity states of passive scalar transport in isotropic turbulence," *Phys. Fluids* **6**, 1036 (1994).
- <sup>9</sup>J. R. Chasnov, "The decay of axisymmetric homogeneous turbulence," *Phys. Fluids* **7**, 600 (1995).
- <sup>10</sup>J. R. Chasnov, "Some similarity states of stably-stratified homogeneous turbulence," to be published in *Dyn. Atmos. Oceans* (1995).
- <sup>11</sup>K. D. Squires, J. R. Chasnov, and N. N. Mansour, "On the asymptotic similarity of rotating homogeneous turbulence," *Proceedings of the 1994 Summer Program of the Center for Turbulence Research* (1994).
- <sup>12</sup>J. R. Chasnov and R. S. Rogallo, "Generation of large-scale density fluctuations by buoyancy," *Proceedings of the 1990 Summer Program of the Center for Turbulence Research* (1990).
- <sup>13</sup>J. R. Chasnov, "Computation of the Loitsianski integral in decaying isotropic turbulence," *Phys. Fluids A* **5**, 2579 (1993).
- <sup>14</sup>M. Lesieur, *Turbulence in Fluids* (Kluwer Academic, Dordrecht, 1990).
- <sup>15</sup>R. S. Rogallo, "Numerical experiments in homogeneous turbulence," NASA Tech. Memo. TM 81315, 1981.
- <sup>16</sup>A. Wray and R. S. Rogallo (private communication).
- <sup>17</sup>R. H. Kraichnan, "Eddy viscosity in two and three dimensions," *J. Atmos. Sci.* **33**, 1521 (1976).
- <sup>18</sup>J. P. Chollet and M. Lesieur, "Parameterization of small scales of three-dimensional isotropic turbulence utilizing spectral closures," *J. Atmos. Sci.* **38**, 2747 (1981).